Adaptive Power Quality Management Using an Optimum and Intelligent Shunt Active Power Filter Conditioner System

Basim Mohammed A. Anwer and Ahmed Nasser B. Alsammak *

Posted Date: 11 May 2026

doi: 10.20944/preprints202605.0554.v1

Keywords: fuzzy gain scheduling; non-linear loads; power quality management; harmonic mitigation; reactive power compensation; FACTS; STATCOM; shunt active power filter; Shunt Active power filter conditioner; whale optimization algorithm

 doi:10.20944/preprints202605.0554.v1

Article

Adaptive Power Quality Management Using an Optimum and Intelligent Shunt Active Power Filter Conditioner System

Basim Mohammed A. Anwer and Ahmed Nasser B. Alsammak *

Department of Electrical Engineering, College of Engineering, University of Mosul, Mosul 41001, Iraq

* Correspondence: ahmed_alsammak@uomosul.edu.iq.

Abstract

A serious problem facing power systems today is the deterioration of power quality (PQ), driven mainly by the widespread use of non-linear loads, such as power electronic converters and adjustable-speed drives. These loads inject harmonic currents into the network, resulting in voltage distortion, increased losses, overheating, and reduced system efficiency. Therefore, harmonic mitigation and reactive power compensation are necessary to ensure stable and reliable operation. This paper presents the development of a Shunt Active Power Filter (SAPF) to become an intelligent Shunt Active Power Filter Conditioner (SAPFC) that operates under different loading conditions (linear, non-linear, or mixed). As a result, a conventional PI controller is upgraded with a Fuzzy Gain Scheduling (FGS) technique optimized by Whale Optimization Algorithm (WOA) in order to keep the DC-link capacitor voltage stable. In addition, an adaptive instantaneous dq theory is used to produce accurate reference currents. The proposed intelligent SAPFC is implemented and validated in MATLAB-Simulink, where simulation results show that it maximizes SAPFC effectiveness by minimizing harmonic distortion to less than 0.7% and achieving a near-unity power factor under different operating conditions. The integrated SAPFC, with its intelligent control, offers a robust and adaptive solution for improving power quality in modern electrical systems, thereby increasing efficiency and reducing power losses.

Keywords: fuzzy gain scheduling; non-linear loads; power quality management; harmonic mitigation; reactive power compensation; FACTS; STATCOM; shunt active power filter; Shunt Active power filter conditioner; whale optimization algorithm

1. Introduction

The increasing prevalence of non-linear loads in contemporary power systems has exacerbated power quality (PQ) issues. These encompass a spectrum of phenomena, including voltage sags, voltage swells, harmonic distortion, transient events, and frequency deviations. The most significant manifestation of harmonics produced by non-linear loads is frequently observed at the Point of Common Coupling (PCC) [1]. Further, contributes to system losses. Even with linear loads, a suboptimal power factor and power flow increase losses and reduce grid stability. Such PQ disturbances can damage or cause malfunctions in sensitive equipment, thereby contributing to overall system losses and negatively impacting operational efficiency and reliability [2,3]. In recent years, researchers and academics have shown heightened interest in enhancing shunt active power filters (SAPF), static synchronous compensators (STATCOM), unified power flow controllers (UPFC), unified power quality controllers (UPQC), and other Flexible AC Transmission Systems (FACTS) [4,5]. The growing demand for electrical power requires an augmentation of reactive power. STATCOM, a second-generation FACTS device, has significantly influenced the electricity sector since the 1980s. STATCOM technology efficiently addresses this issue by improving the efficiency and stability of AC transmission networks [6]. The following individuals created the device: In 2000,

 doi:10.20944/preprints202605.0554.v1

Rao et al. examined the efficacy of state-feedback control approaches for STATCOMs in power systems, specifically for voltage regulation. It evaluates the efficacy of state-feedback control techniques against traditional PI controllers in STATCOM operation. The research indicates that state feedback control approaches have enhanced performance in response dynamics and control effort compared with PI controllers [7]. In 2014, Al-Ismail et al. investigated how coordinating Power System Stabilizers (PSS) and STATCOM stabilizers could improve power system stability. They looked at how gain and phase modulation affected the design of STATCOM damping controllers and found that differential evolution improved it. As nonlinear simulations show, the suggested damping stabilizers perform well in a real-time digital simulator [8]. In 2018, Ahmadinia et al. proposed a coordination strategy for ULTC and STATCOM to efficiently regulate voltage and reactive power. STATCOM delivers rapid voltage regulation, but ULTC functions more slowly, resulting in coordination challenges and excessive STATCOM consumption. The suggested method changes STATCOM control while keeping ULTC functionality. This prevents overuse of the STATCOM and maintains reserve capacity for emergencies. The simulation findings confirm the efficacy and precision of the suggested coordination mechanism [9]. The number of non-linear loads is growing, so power harmonics in electrical grids will increase, causing several issues in electrical devices, including elevated low power factors that generate reactive power, increased system losses, and jeopardizing grid stability. This can overheat transformers, potentially causing contact failures. Reactive power also induces LC resonance, worsening the problem. Increased neutral current, another result of low power factor, further contributes to these detrimental effects [3].

Passive filters are employed to mitigate harmonics; their effectiveness is limited, as they cannot fully eliminate all harmonics produced by non-linear loads. They are replaced by active power filters (APFs); they are parallel (SAPF) and series (series APF) . SAPF, which was developed in this study, among those. In 2020, Mishra et al. showed that a SAPF can effectively correct for current harmonics. Diverse control mechanisms are available for SAPF applications. Fractional Order PID (FOPID) controllers surpass traditional PID controllers in performance [10]. A superior approach involves the Multiple Second-Order Generalized Integrators and Frequency-Locked Loop (MSOGI-FLL) method, which Li et al. used in 2020 to make a predictive control strategy for SAPF. The improved MSOGI-FLL effectively isolates active basic current, enhancing resilience to grid disturbances. Hardware-in-the-loop testing shows that this leads to fast dynamics, a unit power factor, and low total harmonic distortion [11]. In 2021, Rath et al. developed model predictive (MP-DPC) and algorithm-based DPC control approaches for SAPF. These solutions mitigate the limitations of classic DPC, providing enhanced power quality and lower THD compared to conventional techniques. Although MP-DPC demonstrates enhanced performance, it requires more processing resources [12]. In 2022, Sivasubramanian et al. addressed power quality issues caused by non-linear loads. A revised multi-level boost ANPC inverter functions as a shunt active power filter. The inverter regulates the connection voltage using a PI controller and an Adaptive Neuro-Fuzzy Inference System (ANFIS). Harmonic extraction with a radial basis function neural network can be employed. The technology achieves a source-current total harmonic distortion of 0.89 %. The simulations are performed using MATLAB and the FPGA Spartan 6E [13].

The unified power flow controller (UPFC), a Flexible AC Transmission System (FACTS) device, regulates both active and reactive power flow on transmission lines. This capability opens new avenues for power regulation and significantly increases the usable capacity of those lines [14]. UPFC generally consists of two parts: Static Synchronous Series Compensator (SSSC) and STATCOM. In 2023, Al-Kaoaz et al. reported that integrating a UPFC into transmission lines directly influences the operation of distance relays because it changes the apparent impedance, which can cause overreach and underreach depending on the device location, reference power settings, and fault type. Simulations computed in MATLAB indicated that variations in reference active and reactive power do affect the impedance as recorded by the relay, and that when the UPFC is located in the middle of the line, it has more effect as compared to the endpoints. As such there is need to use new tripping parameters to ensure the accuracy and reliability of distance protection in recent transmission

 doi:10.20944/preprints202605.0554.v1

network [15]. In 2023, Ghadi et al. explored the challenges of Load Frequency Control (LFC) in modern power systems. It reviews various control strategies, from traditional methods to more advanced techniques. The review includes evaluating optimization methods, such as genetic algorithms and particle swarm optimization, for enhancing LFC performance. Furthermore, the academic works reviewed highlight the growth of UPFC and renewable energy and explore fuzzy logic and ANN regulators [16].

The efficacy of using a unified power quality conditioner (UPQC) in enhancing power quality within electrical grids has increased over the last five years. UPQC combines series and shunt active power filters for effective compensation. Various control strategies for UPQC are discussed in the literature. UPQC's implementation demonstrates improved adaptability and reduced Total Harmonic Distortion (THD) with IEEE Standard 519, thereby increasing efficiency in grid management [17–19].

All previous studies that used SAPF mostly focused on non-linear loads, neglecting the analysis of mixed linear and non-linear stresses. This work proposed a new intelligent type of SAPF with a conditioner, under the name Shunt Active Power Filter Conditioner (SAPFC), that combines the strengths of Shunt Active Power Filters (SAPF) and Static Synchronous Compensators (STATCOM). i.e., combine the shunt part from UPQC with the shunt part from UPFC. The SAPFC utilizes a shared DC-link capacitor and linked inductor to efficiently mitigate harmonics and reactive power from both linear and non-linear loads, resulting in rapid unit power factor dynamics and little total harmonic distortion (THD). The proposed intelligent control included Fuzzy Gain Scheduling (FGS) for the PI controller, designed using the Whale Optimization Algorithm (WOA), yielding a more accurate and robust response. The results were validated by MATLAB-Simulink.

2. Shunt Active Power Filter Conditioner (SAPFC)

The Active Power Filter (APF) will be constructed using a configuration consisting of voltage-source inverters sharing a common DC-link capacitor and a linked inductor. Based on the shunt specifications, this may be integrated into the distribution line. SAPF architecture shares structural similarity with the STATCOM [20].

This paper proposed an integrated SAPFC that combines STATCOM and SAPF functions, as seen in Figure 1. This helps reduce harmonics and fix reactive power for both linear and non-linear loads.

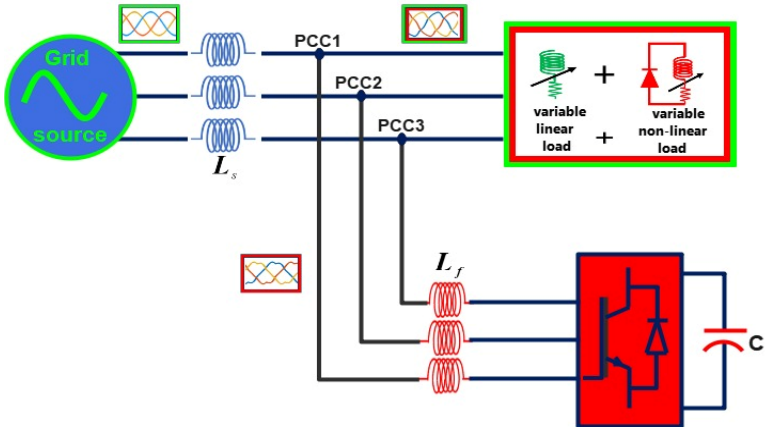

Figure 1. The proposed shunt active power filter conditioner.

This illustrates the concept of initial compensation in the SAPFC. The SAPFC is regulated to either extract or inject compensation. The current through L_f from and to the connecting points (PCC1, PCC2, and PCC3) is meant to eliminate any harmonics or reactive currents on the network side. This ensures that the source side has the SAPFC to generate a pure sinusoidal current perfectly in phase with the voltage. This system utilizes a three-phase voltage source converter (VSC) with

 doi:10.20944/preprints202605.0554.v1

three legs, a capacitor (C), and a three-phase inductor (L_f). SAPFC services address processing difficulties inside the distribution substation, including a range of loads. SAPFC exhibits favorable outcomes for managing linear variable loads, non-linear variable loads, and their mixtures.

This study utilizes the d-q theory to produce reference currents. A control mechanism will be used to monitor these currents. The voltage of the DC connection capacitor is controlled. DC link capacitor voltage regulation utilizes a proportional-integral (PI) controller. The difference between the reference voltage and the actual DC link capacitor voltage is fed into the PI controller. By appropriately tuning its proportional and integral gains, the PI controller maintains the DC link capacitor voltage at the desired reference value. The controller evaluates THD and power factor across several scenarios while adhering to the prescribed limits.

A simulation model was constructed in the MATLAB-Simulink environment. Figure 2 summarizes what SAPFC is and how important it is for balancing out harmonics, reactive power in linear loads, and reactive power in non-linear loads. This significantly raises the power factor and improves power quality. When using SAPF for mass load compensation, it is very important to accurately find the compensating current so that the system can work at its best.

Figure 2. Characteristics of the proposed SAPFC.

3. Mathematical Modelling

In PCC, the magnitude must match the harmonic with the opposite polarity, and reactive current must be added to provide built-in compensation. This thus enhances the quality of strength in distribution systems. The PCC shows how the SAPFC is connected to the power system and how it is set up in its most basic form. In Figure 3, L_f induction facilitates the suppression of harmonics inside the system. The source voltage is denoted (v_s) as follows [21]:

$$v_s\,(t) = Vm\ sin\omega t \tag{1}$$

The geometric relationship (in steady state) defines the interlinked formulations for the non-linear load current (i_{nl}) as follows:

$$i_{nl}(t) = [i_{nl.hn} * \sin\,(n\omega t + \theta_{hn})] \tag{2}$$

Figure 3 illustrates the categorization of the current load data into three distinct components under a non-linear load. A total harmonic component ($i_{nl.hn}$) at various frequencies, together with an active component and a reactive component at the fundamental frequency, as shown below:

$$i_{nl}(t) = [i_{nl.h1} * \cos(\theta_{h1}) * \sin\,(\omega t)] + [i_{nl.h1} * \sin(\theta_{h1}) * \cos\,(\omega t)] + \sum_{n=2}^{\infty}[i_{nl.hn} * sin\,(n\omega t + \theta_{hn})] \tag{3}$$

Let θ_{h1} represent the phase angle at the fundamental frequency while θ_{hn} denotes the phase angle at various harmonic frequencies, where n signifies the order of each respective harmonic.

$$i_{nl}(t) = i_{nl_{active}}(t) + i_{nl_{reactive}}(t) + i_{nl_{harmonic}}(t) \tag{4}$$

The compensating injection currents ($i_{nl_{compensation}}$) required by the SAPFC for a non-linear load are:

 doi:10.20944/preprints202605.0554.v1

$$i_{nl_{compensation}}(t) = i_{nl_{reactive}}(t) + i_{nl_{harmonic}}(t) \quad (5)$$

In a linear load, the load current (i_{ll}) data is split into two separate parts, as shown in Figure 3, an active part and a reactive part at the fundamental frequency.

$$i_{ll}(t) = i_{ll_{active}}(t) + i_{ll_{reactive}}(t) \quad (6)$$

The compensatory currents that the SAPFC must produce with a linear load are:

$$i_{ll_{campensation}}(t) = i_{ll_{reactive}}(t) \quad (7)$$

When linear and non-linear loads are added together, the supplied load current (i_{lnl}) data is divided into five separate parts, as shown in Figure 3. The non-linear load consists of three components: the total harmonic, active, and reactive components, while the linear load consists of two components: the active and reactive components.

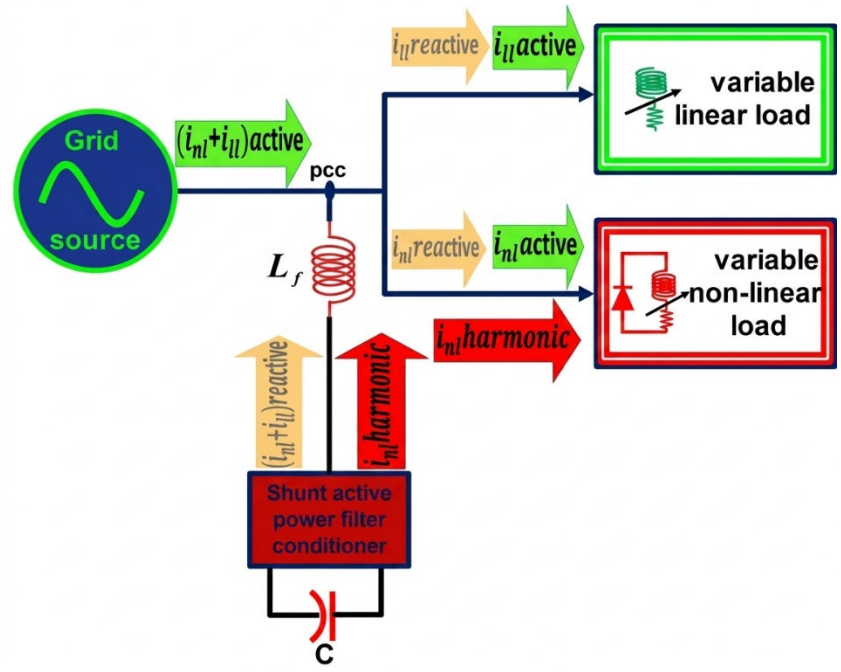

Figure 3. Flow components of load current from the grid Source and SAPFC.

$$i_{lnl}(t) = i_{nl_{active}}(t) + i_{nl_{reactive}} + i_{nl_{harmonic}}(t) + i_{ll_{active}}(t) + i_{ll_{reactive}}(t) \quad (8)$$

The SAPFC must generate the compensating currents ($i_{lnl_{campensation}}$) for a combination of linear and non-linear loads.

$$i_{lnl_{campensation}}(t) = i_{nl_{reactive}}(t) + i_{nl_{harmonic}}(t) + i_{ll_{reactive}}(t) \quad (9)$$

 doi:10.20944/preprints202605.0554.v1

4. SAPFC Current Control

The proposed SAPFC architecture for current control is predicated on a three-phase load current. The load current is measured, identified as its actual component, and transformed into two phases using the d-q technique. Subsequently, the DC voltage regulation signal (PI controller) is added to the d-axis. The system then converts the d-q components back to three-phase and subtracts the current from the initial load. After being subtracted from the SAPFC system, the currents are sent through the hysteresis current controller, which initiates switching the six IGBTs in the VSC, as illustrated in Figure 4. The subsequent sections offer a more in-depth explanation of the control units.

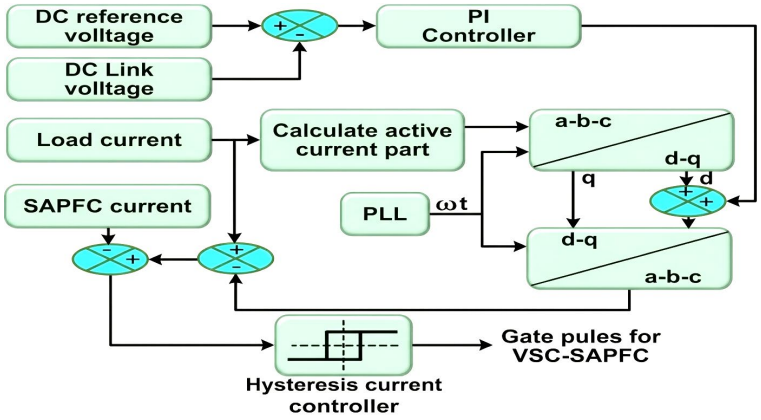

Figure 4. SAPFC current control procedure.

3.1. Calculate the Active Current Part

Active current is the most significant and distinctive feature of the proposed SAPFC system. The benefit of this dependence is evident when the output current is deducted from the initial load current, as when loads are not linear, only the reactive and harmonic parts of the current are made, and when loads are linear, however, only the reactive part is made, and the SAPFC system makes up for it without drawing power from the supply.

3.2. Instantaneous Active and Reactive Current (d-q) Method

A synchronous reference theory is used as a technique to control the DC voltage. As part of synchronous reference theory, the real part of the three-phase load current is changed into a synchronous d-q reference current. This removes the harmonics in the source current and adds the DC voltage to the D-converter. The primary benefit of this approach is that it just considers the load current to provide a reference current. Therefore, it is unaffected by source current and voltage distortion. A distinct PLL block is used to ensure synchronization between the reference and voltage, thereby enhancing system performance. This approach is slower than the d-q method for detecting and eliminating harmonics due to the absence of immediate action. The three stages replace the d-q method [22].

3.3. DC-Link Voltage Control

Figure 4 illustrates DC voltage regulation methods. Whale optimization optimizes K_p and K_i gains for each stage (or case), which are then collected and used to design the FGS for automatically updating the K_p and K_i gains to achieve perfect performance; the PI controller adjusts the DC-link voltage to match the reference and adjusts the d-axis component of the voltage source converter to maintain the target DC-link voltage and reduce power loss. This modification guarantees that the converter extracts the requisite active power from the source.

 doi:10.20944/preprints202605.0554.v1

3.4. Whale Optimization Algorithm (WOA)

Humpback whales, among the biggest cetaceans, exhibit remarkable social characteristics and often inhabit groups. Upon attaining the dimensions of a school bus, these gentle giants mostly consume krill and tiny fish. Their most notable characteristic is the distinctive fishing technique referred to as bubble net feeding. This intricate strategy involves the production of unique bubble structures, often in "9" shapes, to ensnare creatures near the surface, as seen in Figure 5. A new study that used sensor technology found complex underwater movements connected to bubble network feeding, like "biopsy" and "dual rings." These movements give us more information about this complicated activity [23].

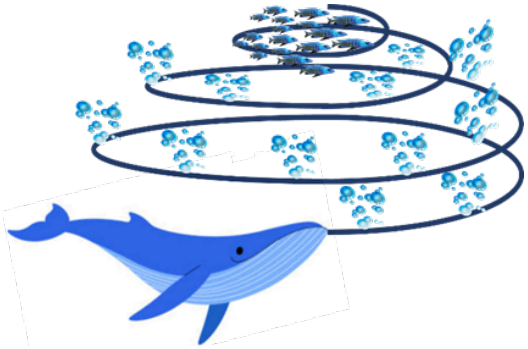

Figure 5. Bubble-net feeding behavior of humpback whales.

An objective function capable of reflecting the dynamic behavior of the system. The Time-Weighted Root Mean Square (TW-RMS) error criterion is employed as an optimization objective to quantitatively evaluate system response quality. By assigning higher weights to errors occurring at later time instants, as shown in Equation (10), this index discourages sustained oscillations and slow convergence, leading to enhanced transient performance and improved steady-state accuracy. The evaluation is performed over the time interval (0-1 s), which represents the critical operating period for controller parameter optimization.

$$F = TW\_RMS \tag{10}$$

The difference between the actual DC-link voltage (Vdc) and the reference voltage (Vdc ref), denoted as the error signal (e). Seven loading scenarios were evaluated and combined to achieve accurate performance in developing a robust controller. Therefore, various loading conditions must be assessed and aggregated to construct a suitable objective function for optimization, as shown in Equation (11). The primary objective of this optimization is to minimize this function.

$$F = F_1 + F_2 + F_3 + F_4 + F_5 + F_6 + F_7 \tag{11}$$

The Whale Optimization Algorithm (WOA) is utilized to minimize the objective function, drawing inspiration from humpback whales' bubble-net hunting. Using conspecific positions for target localization, the whale initiates an encircling maneuver involving two concurrent actions. These movements comprise linear motion along a shrinking circle and circular motion along a spiraled path. As the whale nears its target, it proceeds to hunt. This systematic approach is mathematically structured into three key phases, one of which involves the search for prey. This is referred to as exploration, after which the prey is encircled. Ultimately, hunting behavior is classified as exploitation. This approach optimizes the unknown parameters (K_p and K_i) of the PI controller by minimizing the objective function. It shows where the prey is, while the unknown PI controller's K_p and K_i show the whale. The objective is to determine values for K_p and K_i that minimize the produced function (F). In the first step of the whale optimization process, the population of whales is set to a certain number of sets for the parameters K_p and K_i. The whales' positions are set randomly,

 doi:10.20944/preprints202605.0554.v1

as indicated by the random values for K_p and K_i assigned in every set. The motion of each whale towards the fish group is determined by evaluating its propriety. Proximity to the fish group, and every whale adjusts its location in relation to the optimal one. Following the position update for each search agent, a fitness evaluation is performed. Subsequently, the agent exhibiting the lowest fitness value is identified and designated as the optimal search agent. As previously mentioned, whales use two motions to adjust their posture toward the prey after determining its location. For p ≤ 0.5, the best optimal agent distance defines the circular trajectory, with the equation shown.

$$\overrightarrow{X(t+1)} = \overrightarrow{D'}.e^{-bL}.\cos 2\pi L + \overrightarrow{X^*}(t) \tag{12}$$

Where here $\overrightarrow{D'} = \left|\overrightarrow{X^*}(t) - \vec{X}(t)\right|$, b represents a constant that influences the shape of the search space. L is a stochastic variable uniformly distributed within the interval [-1, 1], $\overrightarrow{X^*}(t)$ denotes the optimal search agent identified at time t.

If $p \geq 0.5$, a linear trajectory ensues; a coefficient, A, is defined as linearly decreasing in magnitude. If the coefficient A>1, a random whale location is selected, and updated positions transition from 2 to 0.

$$\vec{D} = \left|\vec{C}.\overrightarrow{X_{rand}(t)} - \overrightarrow{X(t)}\right| \tag{13}$$

$$\overrightarrow{\mathrm{X}}(\mathrm{t}+1) = \overrightarrow{\mathrm{X}_{\mathrm{rand}}(\mathrm{t})} - \vec{\mathrm{A}}.\vec{\mathrm{D}} \tag{14}$$

Where $\overrightarrow{X_{rand}(t)}$is a random search agent chosen from the present community $\overrightarrow{X}$ and $\vec{C}$ is a coefficient defined as $\vec{C} = 2 * rand$. Coefficient A value is determined via:

$$\vec{A} = 2 * \vec{a} * \overrightarrow{rand} - \vec{a} \tag{15}$$

Where rand represents a random number. If the coefficient A is less than 1, the agent with the best minimum function is utilized to update the position and is expressed by:

$$\vec{D} = \left|\vec{C}.\overrightarrow{X_{rand}(t)} - \overrightarrow{X(t)}\right| \tag{16}$$

$$\overrightarrow{X}(t+1) = \overrightarrow{X_{rand}(t)} - \vec{A}.\vec{D} \tag{17}$$

After every update, the property is evaluated; if any inspect agent exhibits a lower function, it becomes the optimal search agent. The location of each update agent is verified prior to this occurrence. If any updated agent exceeds the search space, it retains its previous position. When the coefficient equals 0, the whale optimally captures its prey, showing that WOA approaches the optimal solution for the PI controller [24].

3.5. Hysteresis Control

The hysteresis control technique is favoured for its rapid dynamic reaction, current-limiting capabilities, and straightforward application. The reference current and filtered current are compared, and the resulting error signal is fed to the hysteresis controller. The controller emits a pulse width modulation signal instructing a three-phase converter to generate a waveform resembling the identified harmonic waveform, but with the phase altered to eliminate any harmonics in the system. Figure 6 shows hysteresis bounds, +H/-H, that define switching behaviour. Error below

 doi:10.20944/preprints202605.0554.v1

-H triggers output increase (1); above +H, output decreases (0). Within bounds, output remains constant until reversal. Simultaneous same-leg switch activation is prohibited [25].

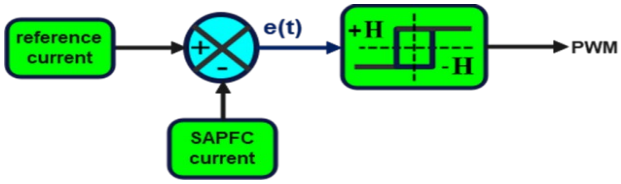

Figure 6. Hysteresis control for VSC switching.

3.6. Fuzzy Logic Controllers

Fuzzy logic controllers (FLCs) have attracted significant attention as a viable choice in various power electronics applications. Their benefits include robustness, the lack of need for a mathematical model, effectiveness in enhancing system stability, and the capacity to accept non-linearity [26–28]. A new, straightforward fuzzy-logic voltage controller manages the DC-link voltage of the converter. It employs a control technique that integrates both PI control and a fuzzy control system, as depicted in Figure 7. The setup involves two fuzzy logic controllers operating in an indirect manner via Fuzzy Gain Scheduling (FGS). One controller modifies the K_p, and the other modifies the K_i. As inputs, both controllers get Total Harmonic Distortion Load (THD_L) and load current (I_L). The outputs are the optimized K_p and K_i values that they get from Whale Optimization.

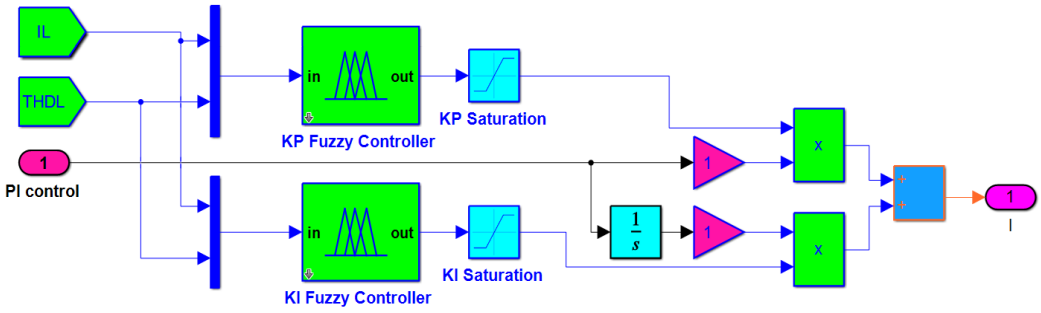

Figure 7. Fuzzy gain scheduling for the DC link PI controller.

4. Simulation, Results, and Discussions

The proposed intelligent SAPFC aims to address both reactive power and current harmonics using a single, comprehensive solution. Rather than using dedicated equipment for harmonic filtering and power factor correction, this strategy aims to achieve its goals. The purpose of this endeavor is to combine both capabilities into a single unit. The use of this integrated solution has potential; In terms of cost, space constraints, control simplicity, and overall system efficiency, so this integrated solution offers several benefits. The fact that it is now in progress indicates that a more streamlined and efficient approach to power quality control is being implemented. Traditional methods tackle harmonics and reactive power separately.

Figure 8 shows the proposed intelligent SAPFC model in MATLAB-Simulink. The system includes a three-phase Voltage Source Converter (VSC) and a series-connected inductor. Figure 9 shows the MATLAB-Simulink test model for the parallel connection between the proposed SAPFC and the medium voltage grid; all model parameters are given in Appendix (A), Table A1. The simulation model used a variety of loads, including linear and nonlinear. To test the SAPFC system, the network was used both before and after compensation. The K_i and K_p values change depending on the FGS, which is created depending on the whale optimization data using Matlab Neuro-Fuzzy Designer, to match different loads.

 doi:10.20944/preprints202605.0554.v1

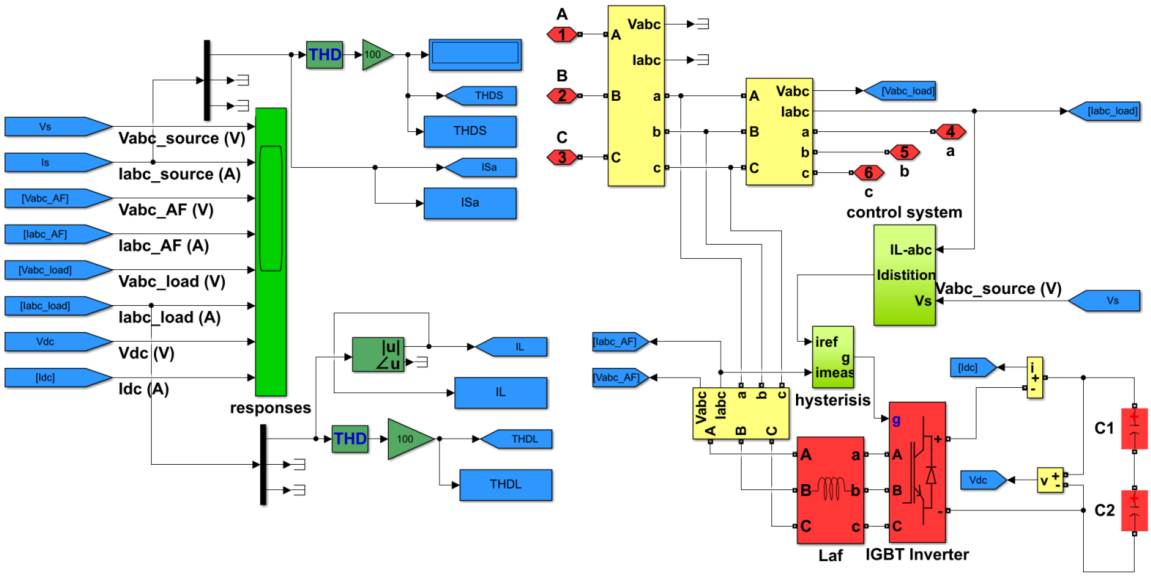

Figure 8. Matlab-Simulink model for the proposed intelligent SAPFC.

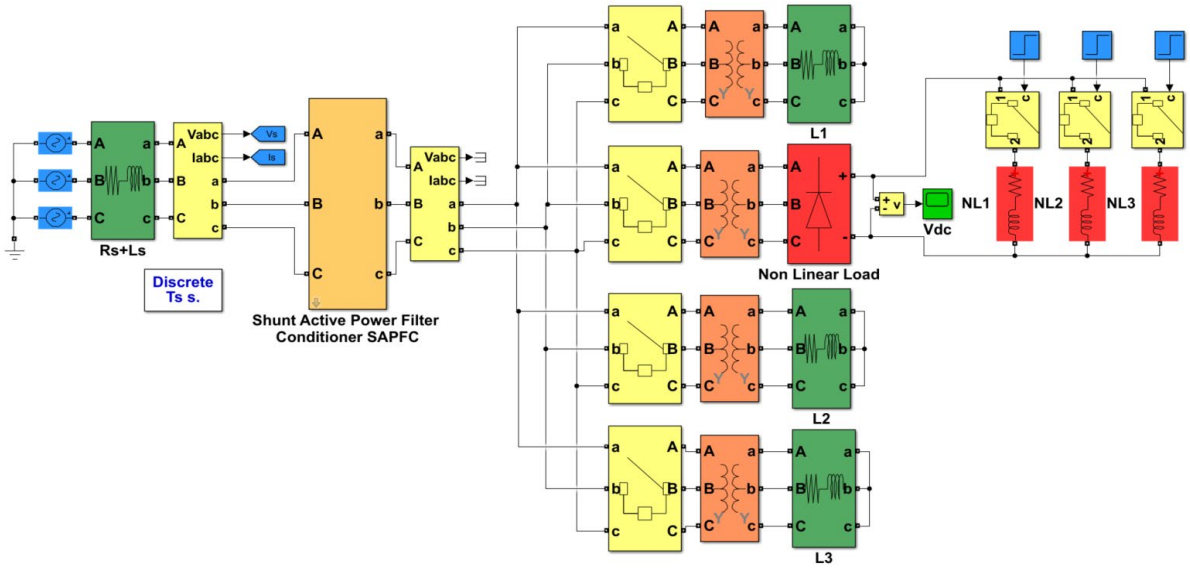

Figure 9. Power grid with the proposed intelligent SAPFC.

4.1. Result of Optimization

The DC voltage loop needs to be specially controlled for operating scenarios where the load conditions are arranged into seven scenarios; the first three scenarios indicate the case of nonlinear load conditions with varying magnitudes, the third and fourth scenarios are mixed linear and nonlinear load cases with varying value, and the final stage is the case of purely linear load. The WAO method adjusts the PI controller's parameters to reduce the objective function. Figure 10 shows these optimization results.

Preprints.org (www.preprints.org) | NOT PEER-REVIEWED | Posted: 11 May 2026 doi:10.20944/preprints202605.0554.v1

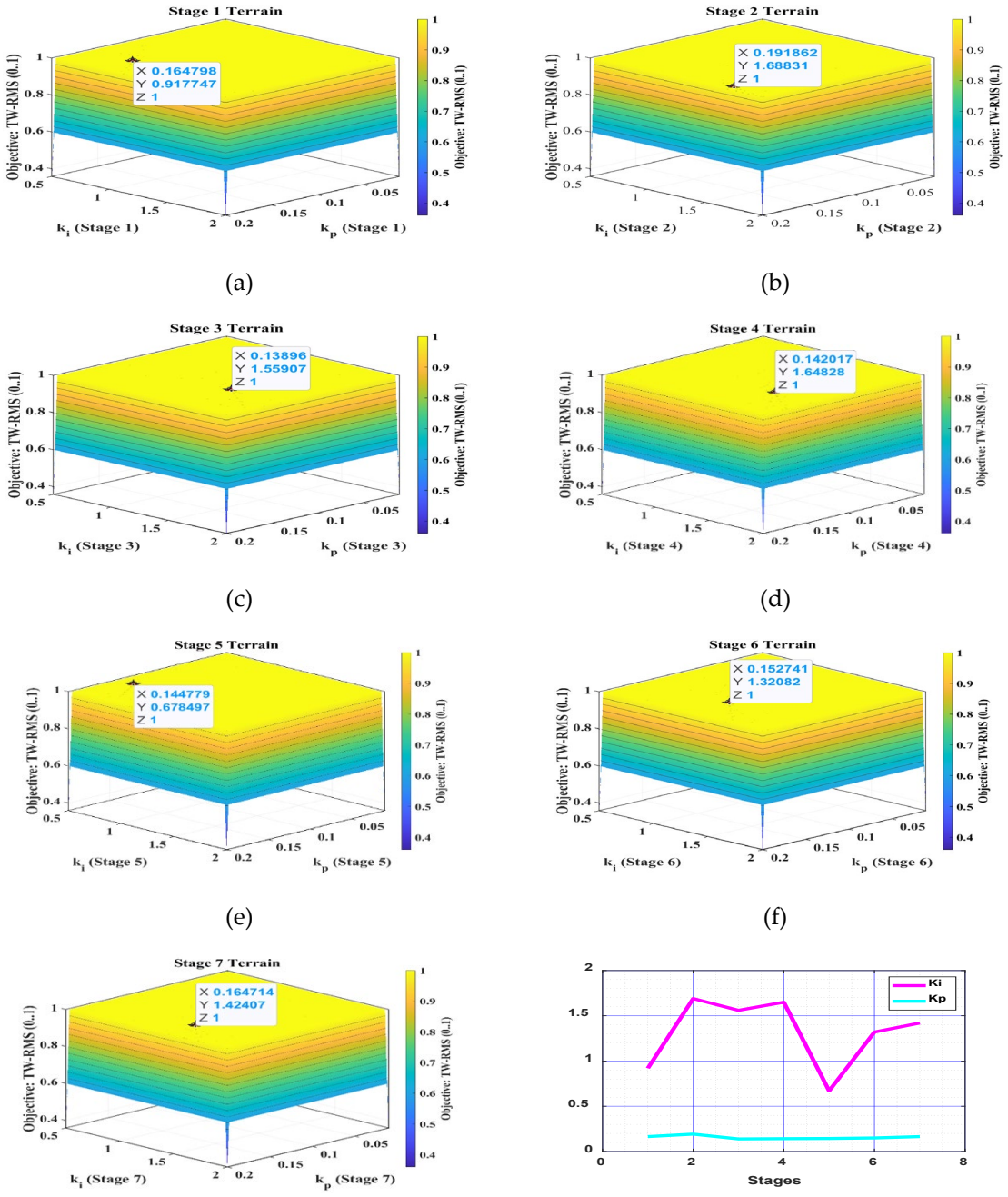

Figure 10. Optimal controller gains (K_p and K_i) for different operating stages: (a) stage 1, (b) stage 2, (c) stage 3, (d) stage 4, (e) stage 5, (f) stage 6, (g) stage 7, and (h) the relationship between K_p and K_i at the seven stages.

The optimum search domain for the K_p and K_i is defined as $0.01 < K_p < 0.5$, $0.5 < K_i < 2$, whereas the search domain for A set of discrete and multiple simulations was performed with the aim of determining the ideal values for the coefficients of the controller K_p and K_i across seven different operational stages. The results showed that the optimal values of each of the K_p and K_i vary from one stage to another, as they are located within the optimal top layer (Z=1). The specific ranges of the target function for each stage are shown in Figure 10. From these results, it was concluded that the K_p value approximately within the limit change, while K_i has a great change due to its contribution to increased stability and elimination of steady-state error. These data were used as an input-output dataset to create a two-input, one-output FGS with Gaussian membership in Neuro-Fuzzy Designer, achieving a training error less than $1*10^{-3}$.

 doi:10.20944/preprints202605.0554.v1

4.2. Result of PI-Based Fuzzy Gain Scheduling Control

The suggested intelligent SAPFC control method was tested through a simulation with increasing non-linear loads along with linear loads. The control technique used a seven-stage Fuzzy Gain Scheduling (FGS) mode control to guarantee dynamic responsiveness under various settings. This controller changes the PI controller's K_p and K_i gains, making it give better perfect and fast performance at all seven stages. This flexible approach lets the SAPFC manage things well even when the load changes, which regular control systems can't do. The FGS mode controller clearly demonstrates its efficacy. Figure 11 illustrates the operation flowchart of the proposed fuzzy system.

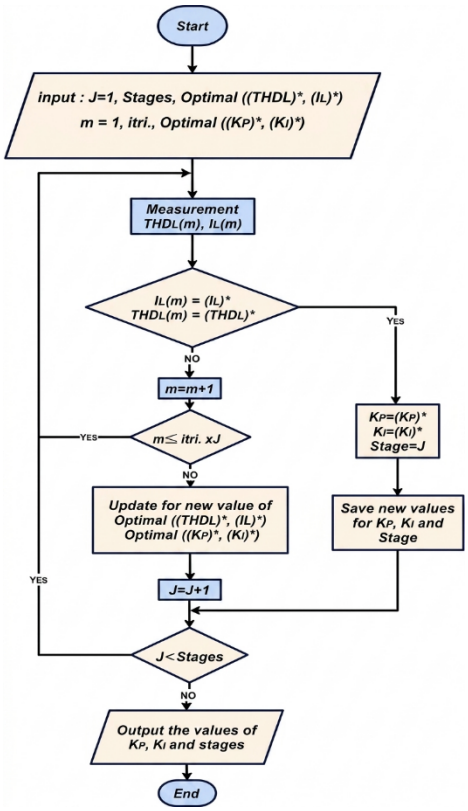

Figure 11. Flowchart of the FGS system.

4.3. Result of the Test Response with SAPFC

A waveform under three-stage non-linear loading conditions that applies to source current prior to the application of SAPFC is seriously distorted, as seen in Figures 12a,c,e. Following compensation, the current waveform is almost a sinusoid and meets IEEE-519 requirements as in Figure 12b,d,f.

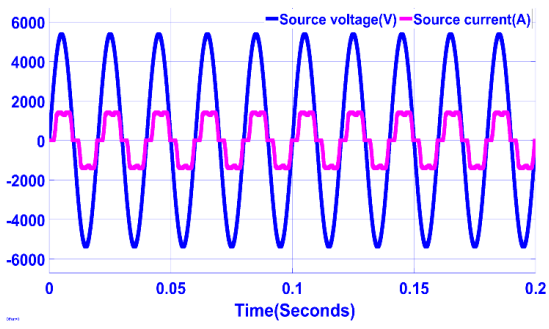

(a)

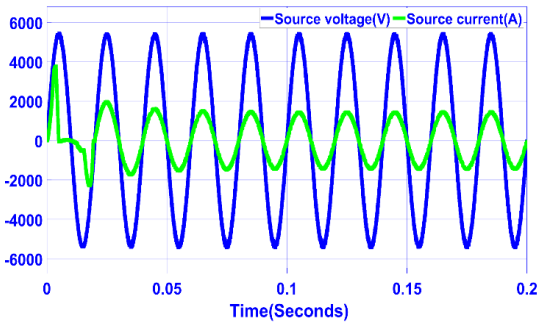

(b)

 doi:10.20944/preprints202605.0554.v1

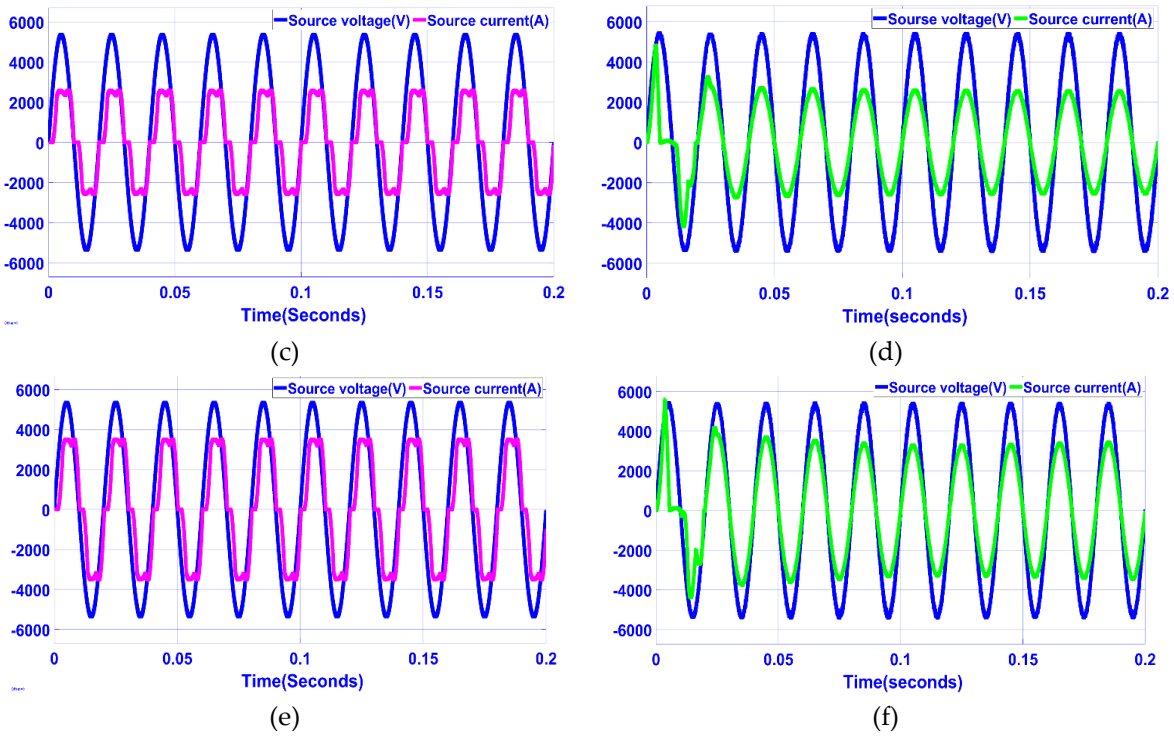

Figure 12. Voltage and current source with nonlinear load:(a) stege1 without SAPFC, (b) stege1 with SAPFC, (c) stege2 without SAPFC, (d) stege2 with SAPFC, (e) stege3 without SAPFC, (f) stege3 with SAPFC.

Even with the uncompensated cases (Figures 13a, 13c, and 13e) applied to the uncompensated case under both linear and non-linear load testing conditions, it can be observed that the waveform distortion is noticeable, but the results shown in Figures 13b, 13d and 13f (compensated) are significantly better, and the source current is now returned to near sinusoidal values and complies with the IEEE-519 standards. In the case of purely linear load, the waveform is actually sinusoidal in nature, and Figure 14a shows operation without SAPFC, and Figure 14b shows operation with SAPFC, which confirms that the compensator matches the quality of the waveform without violating the accepted standards of harmonic limits.

FFT analysis results for the source current under three-phase nonlinear loads show high harmonic distortion when SAPFC is not used, as in Figures 15a, 15c, and 15e, where the THD value increases due to the multiplicity of harmonic components. After compensation, Figures 15b, 15d, and 15f show a clear reduction in harmonics, making the current close to sinusoidal and compliant with the IEEE-519 standard. For combined loads (linear and nonlinear), Figures 16a, 16c, and 16e show high distortion levels before compensation, while Figures 16b, 16d, and 16f show a noticeable improvement and reduced THD after using the filter. For the pure linear load, Figure 17a shows a natural reduction in harmonics, while Figure 17b shows that SAPFC maintains current quality within standard limits.

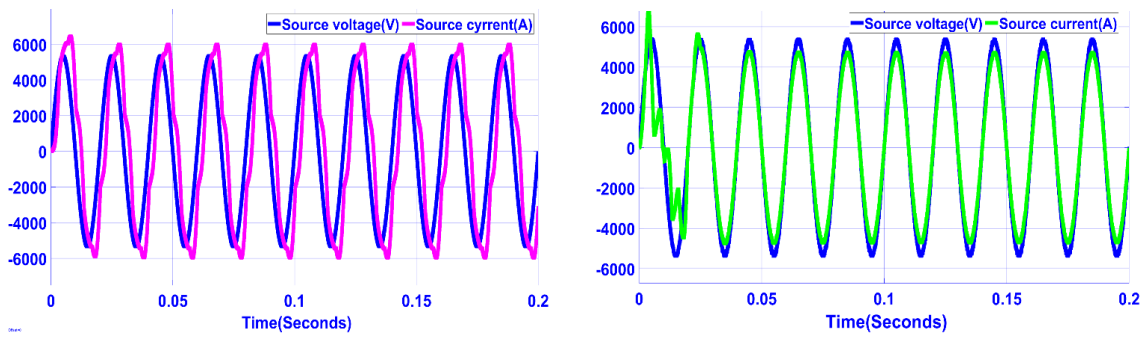

 doi:10.20944/preprints202605.0554.v1

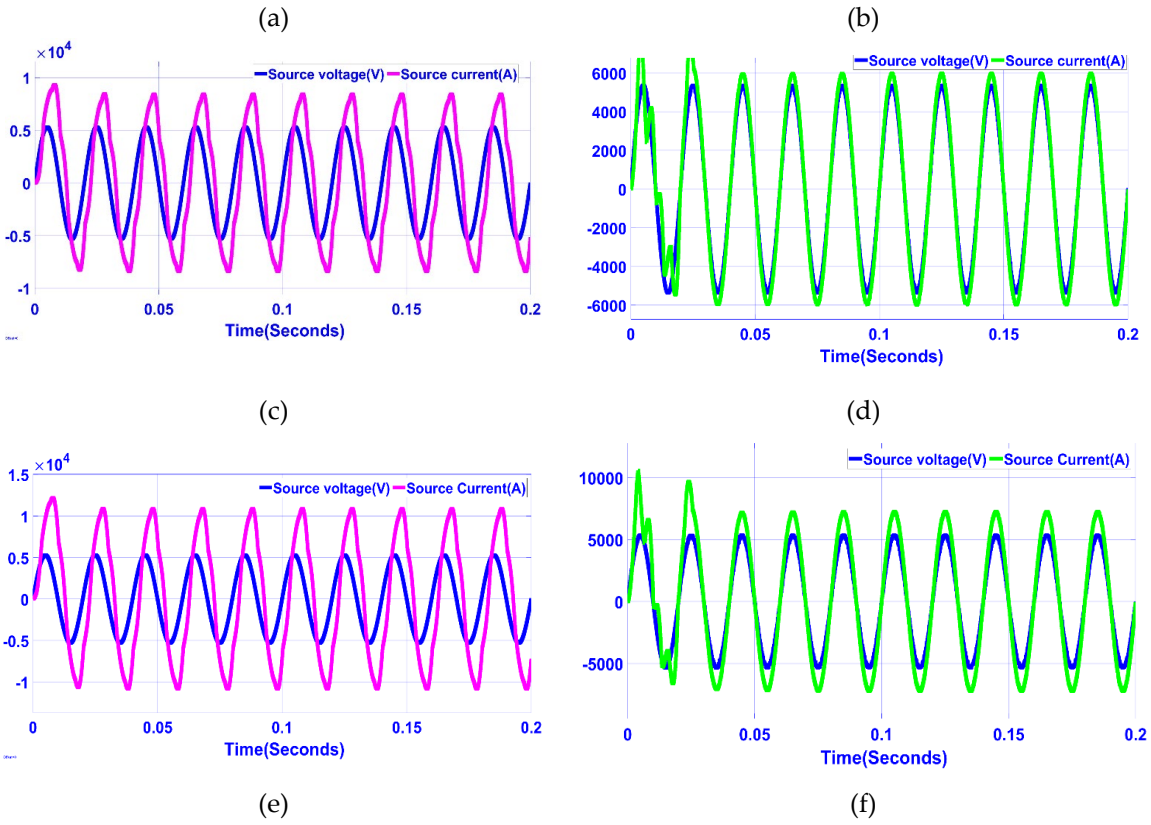

Figure 13. Voltage and current source with linear and nonlinear load:(a) stege4 without SAPFC, (b) stege4 with SAPFC, (c) stege5 without SAPFC, (d) stege5 with SAPFC, (e) stege6 without SAPFC, (f) stege6 with SAPFC.

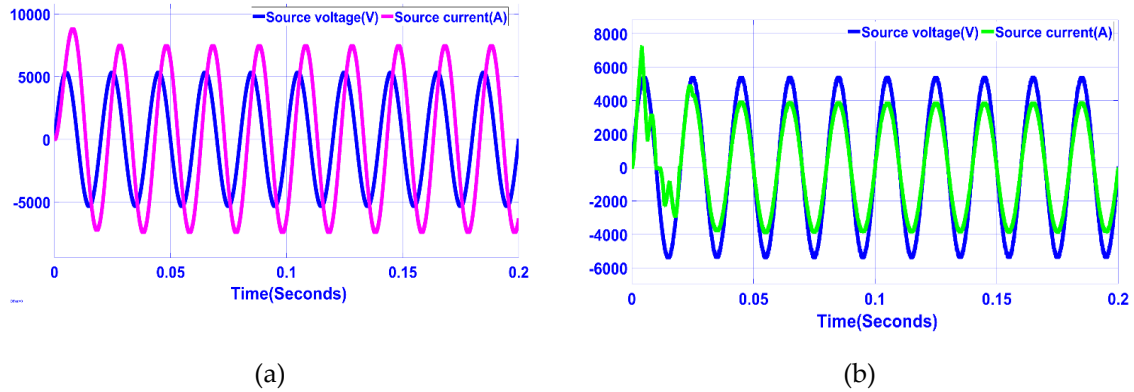

Figure 14. Voltage and current source with linear load (stage7):(a) without SAPFC, (b) with SAPFC.

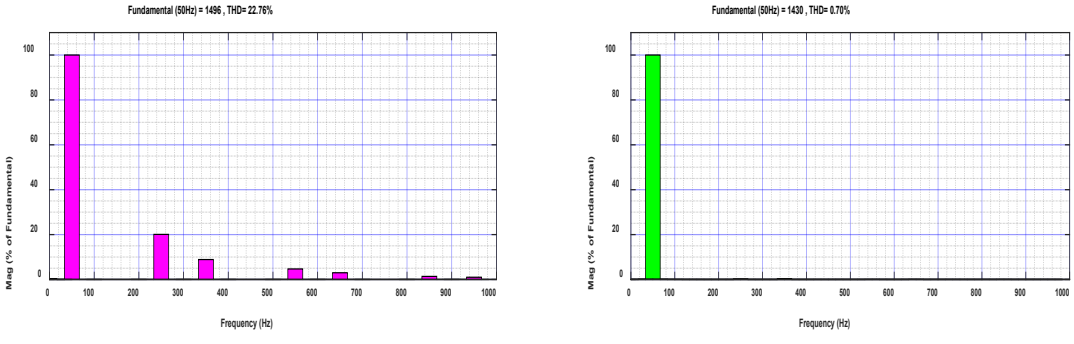

 doi:10.20944/preprints202605.0554.v1

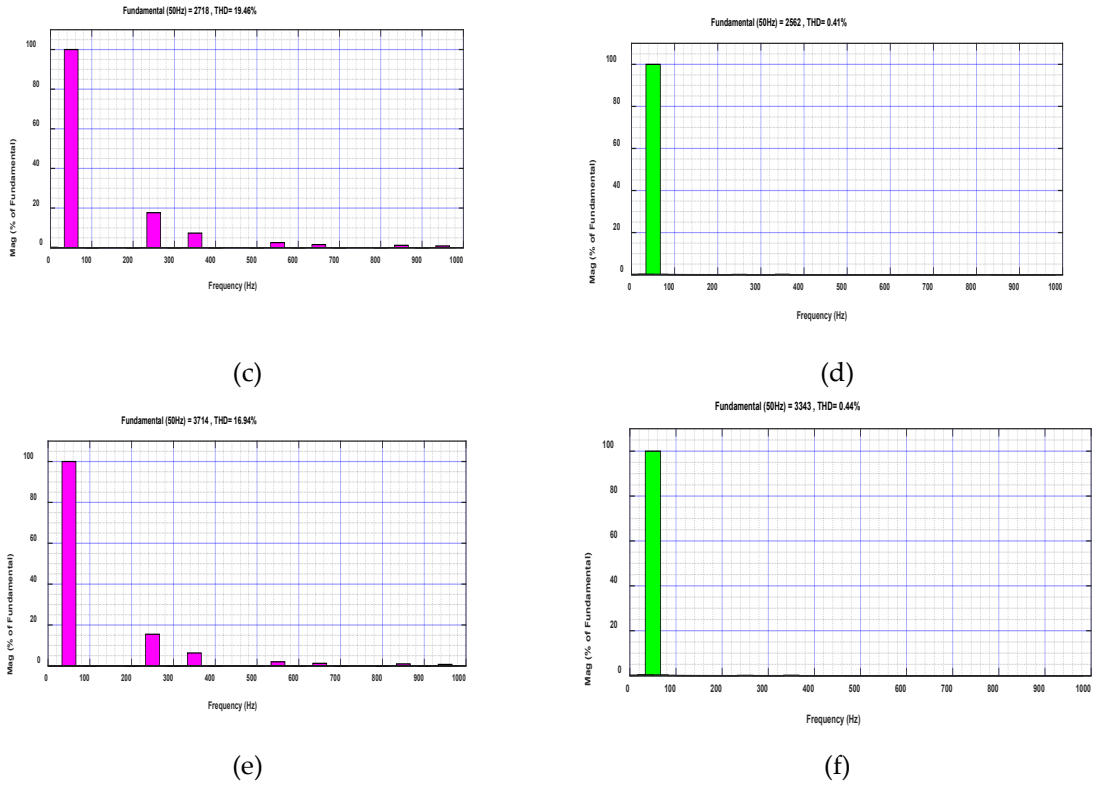

Figure 15. FFT of current source with nonlinear load:(a) stege1 without SAPFC, (b) stege1 with SAPFC, (c) stege2 without SAPFC, (d) stege2 with SAPFC, (e) stege3 without SAPFC, (f) stege3 with SAPFC.

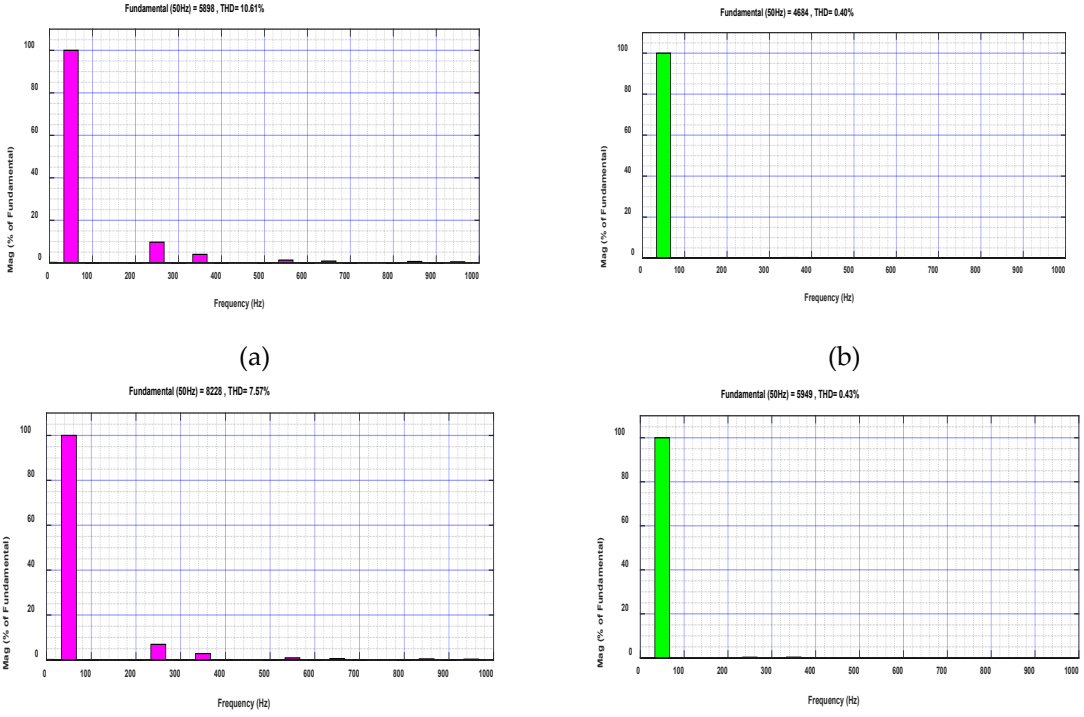

 doi:10.20944/preprints202605.0554.v1

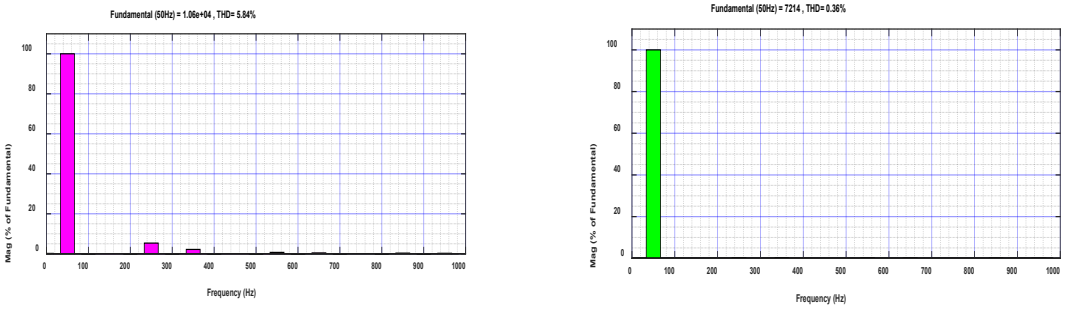

(e) (f)

Figure 16. FFT of current source with linear and nonlinear load:(a) stege4 without SAPFC, (b) stege4 with SAPFC, (c) stege5 without SAPFC, (d) stege5 with SAPFC, (e) stege6 without SAPFC, (f) stege6 with SAPFC.

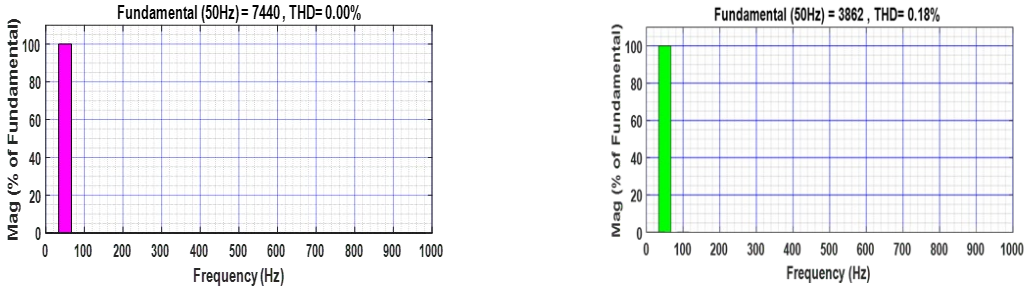

(a) (b)

Figure 17. FFT of current source with linear load (stage7): (a) without SAPFC, (b) with SAPFC.

The simulation results highlight the unit power factor for both linear and non-linear loads, as shown in Table 2, where PF_s denotes the source power factor, which equals the load power factor (PF_L) before compensation. This control is based on the FGS on the PI controller. It has been tested under seven different operating conditions (stages) to assess its performance. The primary performance metric used was the total harmonic distortion (THD) of the current under varying load conditions, which remained below 5% as required. Table 3 displays the values of THD_L, which denotes the source current before compensation, and THD_s, which indicates the source current subsequent to compensation.

Table 2. Power factor before and after compensation.

Stage	Load	PF_L Before	PF_S After
1	NL1	0.9172	0.9998
2	NL1+NL2	0.9032	0.9999
3	NL1+NL2+NL3	0.8910	0.9999
4	NL1+NL2+NL3+L1	0.7824	0.9999
5	NL1+NL2+NL3+L1+L2	0.7155	0.9999
6	NL1+NL2+NL3+L1+L2+L3	0.6740	0.9999
7	L1+L2+L3	0.5142	0.9999

Table 3. Current source THD before and after compensation.

Stage	Load	THD_L% Before	THD_s% After
1	NL1	22.76	0.7
2	NL1+NL2	19.46	0.41
3	NL1+NL2+NL3	16.94	0.44

 doi:10.20944/preprints202605.0554.v1

4	NL1+NL2+NL3+L1	10.61	0.40
5	NL1+NL2+NL3+L1+L2	7.57	0.43
6	NL1+NL2+NL3+L1+L2+L3	5.84	0.36
7	L1+L2+L3	0.00	0.18

The SAPFC system marks a significant leap forward in power quality management, providing a promising solution to the detrimental effects of both linear and non-linear loads. Its effectiveness hinges on an intelligent control strategy that synergistically blends the strengths of fuzzy logic, which works as FGS, PI control, and the Whale Optimization Algorithm (WAO). This integrated approach yields robust and adaptive performance, crucial in modern power systems characterized by fluctuating loads and the growing prevalence of power electronics. At the heart of the SAPFC's intelligence lies its fuzzy logic system. Unlike conventional control methods with fixed parameters, fuzzy logic empowers the system to adapt dynamically to changing load conditions. By monitoring key system variables like voltage, current, and power factor, the fuzzy controller infers the system's current state. It then uses a set of predefined rules to adjust the PI controller's parameters (K_p and K_i) in real time. This adaptability is essential for maintaining optimal performance across diverse operating scenarios, including sudden load changes, the introduction or removal of non-linear loads, and variations in the supply voltage.

The fuzzy logic system's ability to handle uncertainty and imprecise information makes it particularly well-suited to the complex and dynamic nature of modern power grids. This real-time adaptation ensures the SAPFC continuously provides the necessary compensation for harmonics and reactive power, maintaining high power quality regardless of load variations.

Figure 18. shows the online FGS-optimum PI controller values for the proposed intelligent SAPFC when the seven-stage scenarios are applied to the sample test system. This specific selection facilitates a quick, dynamic response to fluctuating load conditions. Seven load-change phases occur, each lasting 0.2 seconds, highlighting the controller's capacity to react swiftly and efficiently to sudden changes in the system's operating conditions. This swift adaptation highlights the advantages of the FGS methodology in managing dynamic systems.

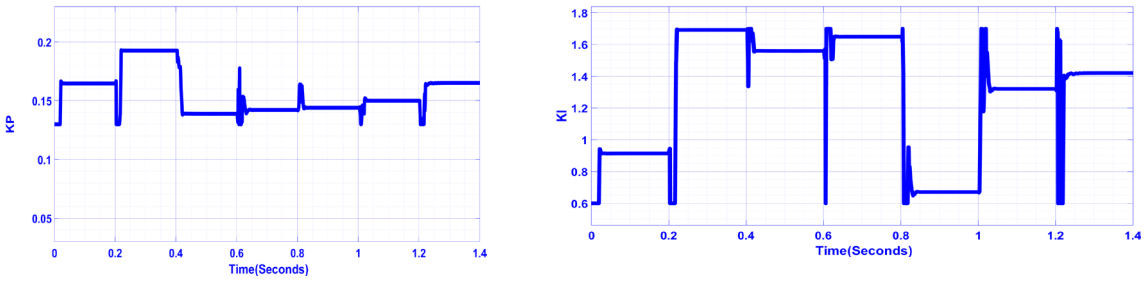

(a) (b)

Figure 18. Output FGS during the system test under the seven stages: (a) K_p (b) K_i.

Figure 19 presents the performance of the proposed intelligent SAPFC system over a 1.4-second interval, subdivided into seven 0.2-second segments. The Figure details voltage and current measurements for the source, load, SAPFC system, and DC link across seven distinct operational stages, encompassing both individual and combined configurations. Critically, the sinusoidal waveform of the source current is illustrated. The integration of Fuzzy Logic Control (FLC) with "p-q theory" in Shunt Active Power Filter (SAPF) systems significantly enhances harmonic reduction and reactive power compensation under both nonlinear and linear load conditions, outperforming traditional PI controllers and conventional methods like standard PWM. System efficiency, evaluated within a consensus processor framework, demonstrates robust responsiveness to network variations across all operational scenarios, as evidenced by the data in Table 3, which shows marked improvements in Total Harmonic Distortion (THD). Furthermore, the DC-link voltage remains stable

 doi:10.20944/preprints202605.0554.v1

and exhibits a rapid transient response in FGS Mode, ensuring reliable performance amid fluctuating loads and network dynamics.

This approach not only achieves superior voltage regulation compared to conventional controls but also underscores FGS's adaptability and effectiveness in addressing complex power quality challenges for both nonlinear and linear load conditions.

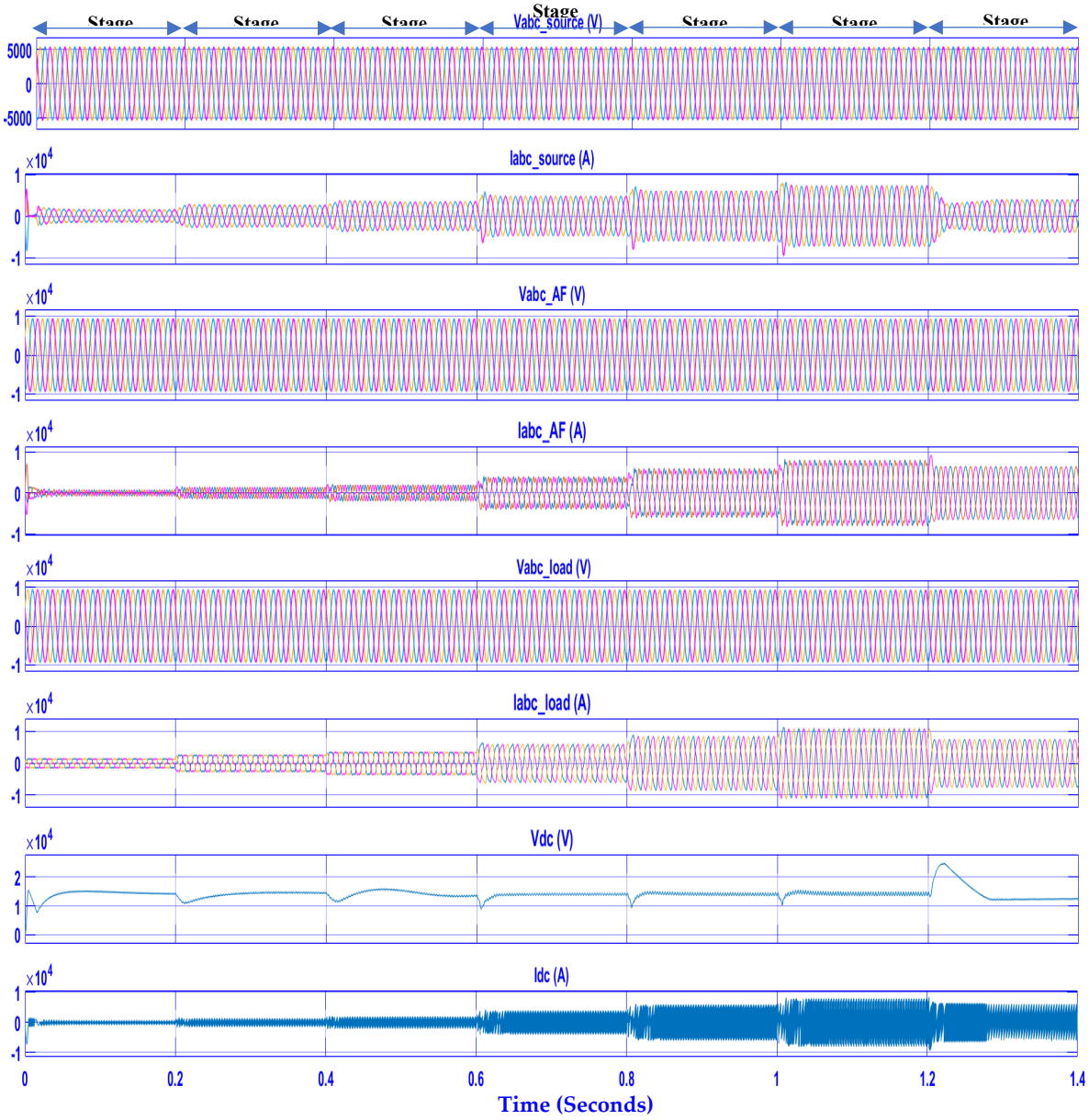

Figure 19. Compensation for reactive power and harmonic under variables, linear and nonlinear loads.

5. Conclusions

This research has introduced the design and execution of an SAPFC to improve power quality in systems with linear and non-linear loads. The SAPFC efficiently addresses harmonic distortion and reactive power compensation using an integrated method, providing benefits in cost, space, and control simplicity over conventional, separate approaches. The core of the SAPFC's performance lies in its intelligent control strategy, which combines the strengths of fuzzy logic, PI control, and the Whale Optimization Algorithm (WAO). Fuzzy logic enables dynamic adaptation of the PI controller gains (K_p and K_i) to varying load conditions, ensuring rapid response and stability. The WAO optimizes these gains, maximizing the SAPFC's effectiveness in minimizing harmonic distortion less

 doi:10.20944/preprints202605.0554.v1

than 0.7% and achieving a near-unity power factor. Simulation results, including FFT analysis and THD measurements, demonstrate the SAPFC's ability to reduce harmonics to within IEEE-519 standards and correct power factors for both linear and non-linear loads. The system's dynamic performance is further validated by its ability to respond quickly and efficiently to sudden load changes across seven different operating stages. The integrated SAPFC, with its intelligent control, offers a robust and adaptive solution for improving power quality in modern electrical systems, thereby increasing efficiency and reducing power losses.

Author Contributions: Conceptualization, B.M.A. and A.N.A.; methodology, B.M.A.; software, B.M.A. and A.N.A.; validation, B.M.A., and A.N.A; formal analysis, A.N.A.; investigation, B.M.A; resources, A.N.A.; data curation, B.M.A.; writing—original draft preparation, B.M.A; writing—review and editing, B.M.A; visualization, B.M.A.; supervision, A.N.A; project administration, A.N.A.; funding acquisition, B.M.A. All authors have read and agreed to the published version of the manuscript.

Funding: This research received no external funding.

Acknowledgments: The authors would like to thank the Department of Electrical Engineering at the College of Engineering, University of Mosul (https://www.uomosul.edu.iq), Mosul, Iraq, for their support of this work.

Data Availability Statement: Data is available to anyone who needs it, just cite it.

Conflicts of Interest: The authors declare no conflicts of interest.:

Abbreviations

The following abbreviations are used in this manuscript:

PQ	Power Quality
SAPF	Shunt Active Power Filter
SAPFC	Shunt Active Power Filter Conditioner
FGS	Fuzzy Gain Scheduling
WOA	Whale Optimization Algorithm
STATCOM	Static Synchronous Compensator
PCC	Point of Common Coupling
FOPID	Fractional Order PID
MSOGI-FLL	Multiple Second-Order Generalized Integrators and Frequency-Locked Loop
MP-DPC	Model Predictive-Direct Power Control
ANPC	Active Neutral Point Clamped
ANFIS	Adaptive Neuro-Fuzzy Inference System
LFC	Load Frequency Control
FACTS	Flexible AC Transmission Systems
UPFC	Unified Power Flow Controller
UPQC	Unified Power Quality Conditioner
SSSC	Static Synchronous Series Compensator
THD	Total Harmonic Distortion
VSC	Voltage Source Converter
ANN	Artificial Neural Network
TW-RMS	Time-Weighted Root Mean Square
v_s	Source Voltage
i_{nl}	Non-Linear Load Current
$i_{nl.hn}$	Current with a Harmonic Component at Various Frequencies, together with an Active Component and a Reactive Component at the Fundamental Frequency.
θ_{h1}	Phase Angle at the Fundamental Frequency
θ_{hn}	Phase Angle at Various Harmonic Frequencies
n	The Order of the Harmonic.
$i_{nl_{compensation}}$	Compensating Injection Currents Required by the SAPFC for a Non-Linear Load
i_{ll}	Linear Load Current
$i_{lnl_{campensation}}$	Compensating Currents Generated by SAPFC for the Linear and Non-Linear Loads
i_{lnl}	The Current Supplied to the Load

 doi:10.20944/preprints202605.0554.v1

PFL	Load Power Factor
PFS	Source Power Factor
THDL	Total Harmonic Distortion of the Load
THDS	Total Harmonic Distortion of the Source
NL1, NL2, NL3	Nonlinear Load1, Nonlinear Load2, Nonlinear Load3
L1, L2, L3	Linear Load1, Linear Load2, Linear Load3

Appendix A

This appendix contains Table A1, which gives details of the parameters used in the test system.

Table A1. Parameters of the test system.

Parameters	Value
Supply Voltage	6600V
Load supply voltage	6600V
Frequency	50Hz
Rs, Ls Source	0.01 Ω, 1e-5 H
R, L Non-linear Load (NL)	6 Ω, 3e-3 H
R, L Linear Load (L)	1 Ω, 0.5e-3 H
L For 3-Φ SAPFC	1e-3 H
C_1 , C_2 DC Capacitor	2.5e-3 F
DC-link voltage	14000V
Three single-phase	25e6 VA, 50Hz
Transformers	6600Y/6600Y

Reference

1. Gaiceanu, M.; Epure, S.; Solea, R.C.; Buhosu, R. Power Quality Improvement with Three-Phase Shunt Active Power Filter Prototype Based on Harmonic Component Separation Method with Low-Pass Filter. *Energies* **2025**, *18*. https://doi.org/10.3390/en18030556.
2. Bhukya, D.; D. Ravi Kumar; M. Siva Improved Power Quality in Distribution System with Renewable Energy Sources Integration. *Trans. Energy Syst. Eng. Appl.* **2026**, *6*, 1–15. https://doi.org/10.32397/tesea.vol6.n2.684.
3. SivaramKrishnan, M.; Kathirvel, N.; Kumar, C.; Senjyu, T. Smart Charging Solution for Electric Vehicles: Leveraging Grid Connected Solar PV with UPQC Using HBA- MORARNN Approach. *Energy Reports* **2025**, *13*, 2454–2467. https://doi.org/10.1016/j.egyr.2025.02.004.
4. Anwer, B.M.; Alsammak, A.N. An Integrated Series Active Power Filter Combined with a PV-Battery System Based on a Fuzzy Logic Controller to Enhance Power Quality for Various Linear and Non-Linear Loads. **2026**, 51–62.
5. Dybko, M.; Brovanov, S.; Udovichenko, A. DC-Link Capacitance Estimation for Energy Storage with Active Power Filter Based on 2-Level or 3-Level Inverter Topologies. *Electricity* **2025**, *6*. https://doi.org/10.3390/electricity6010013.
6. Yu, Q.; Li, P.; Liu, W.; Xie, X. Overview of STATCOM Technologies. *Proc. 2004 IEEE Int. Conf. Electr. Util. Deregulation, Restruct. Power Technol.* **2004**, *2*, 647–652. https://doi.org/10.1109/drpt.2004.1338063.
7. Rao, P.; Crow, M.L.; Yang, Z. STATCOM Control for Power System Voltage Control Applications. *IEEE Trans. Power Deliv.* **2000**, *15*, 1311–1317. https://doi.org/10.1109/61.891520.
8. Al-Ismail, F.S.; Hassan, M.A.; Abido, M.A. RTDS Implementation of STATCOM-Based Power System Stabilizers. *Can. J. Electr. Comput. Eng.* **2014**, *37*, 48–56. https://doi.org/10.1109/CJECE.2014.2309323.
9. Ahmadinia, M.; Ghazi, R. Coordinated Control of STATCOM and ULTC to Reduce Capacity of STATCOM. *26th Iran. Conf. Electr. Eng. ICEE 2018* **2018**, 1062–1066. https://doi.org/10.1109/ICEE.2018.8472712.
10. Mishra, A.K.; Das, S.R.; Ray, P.K.; Mallick, R.K.; Mohanty, A.; Mishra, D.K. PSO-GWO Optimized Fractional Order PID Based Hybrid Shunt Active Power Filter for Power Quality Improvements. *IEEE Access* **2020**, *8*, 74497–74512. https://doi.org/10.1109/ACCESS.2020.2988611.

 doi:10.20944/preprints202605.0554.v1

11. Li, Y.; Zhang, Z.; Zhang, Z.; Wang, J.; Kennel, R. Model Predictive Control of a Shunt Active Power Filter with Improved Dynamics under Distorted Grid Conditions. *2020 IEEE 9th Int. Power Electron. Motion Control Conf. IPEMC 2020 ECCE Asia* **2020**, 1033–1037. https://doi.org/10.1109/IPEMC-ECCEAsia48364.2020.9368136.
12. Rath, A.; Srungavarapu, G. New Model Predictive Algorithm DPC Based Shunt Active Power Filters (SAPFs). *ICPEE 2021 - 2021 1st Int. Conf. Power Electron. Energy* **2021**, 3–8. https://doi.org/10.1109/ICPEE50452.2021.9358550.
13. Sivasubramanian, M.; Boopathi, C.S.; Vidyasagar, S.; Kalyanasundaram, V.; Kaliyaperumal, S. Performance Evaluation of Seven Level Reduced Switch ANPC Inverter in Shunt Active Power Filter with RBFNN-Based Harmonic Current Generation. *IEEE Access* **2022**, *10*, 21497–21508. https://doi.org/10.1109/ACCESS.2021.3064715.
14. Sen, D.; Gupta, M.; Shegaonkar, M.; Das, S.; Acharjee, P. Optimal Location Determination of UPFC Based on Techno-Economic Criteria and Security Constraints. *2018 Int. Conf. Power Energy, Environ. Intell. Control. PEEIC 2018* **2018**, 534–539. https://doi.org/10.1109/PEEIC.2018.8665456.
15. Al-Kaoaz, H.N.A.; Alsammak, A.N.B. Performance Enhancement of Distance Relay in Presence of Unified Power Flow Controller. *Int. J. Power Electron. Drive Syst.* **2023**, *14*, 1577–1588. https://doi.org/10.11591/ijpeds.v14.i3.pp1577-1588.
16. Ghadi, Y.Y.; Neamah, N.M.; Hossam-Eldin, A.A.; Alqarni, M.; Aboras, K.M. State-of-the-Art Frequency Control Strategy Based on an Optimal Fuzzy PI-FOPDFλ for SMES and UPFC Integrated Smart Grids Using Zebra Optimization Algorithm. *IEEE Access* **2023**, *11*, 122893–122910. https://doi.org/10.1109/ACCESS.2023.3328961.
17. Nishad, D.K.; Tiwari, A.N.; Khalid, S.; Gupta, S.; Shukla, A. AI Based UPQC Control Technique for Power Quality Optimization of Railway Transportation Systems. *Sci. Rep.* **2024**, *14*, 1–22. https://doi.org/10.1038/s41598-024-68575-5.
18. Qasim, A.Y.; Tahir, F.R.; Alsammak, A.N.B. Utilizing UPQC-Based PAC-SRF Techniques to Mitigate Power Quality Issues under Non-Linear and Unbalanced Loads. *J. Eur. des Syst. Autom.* **2023**, *56*, 823–831. https://doi.org/10.18280/jesa.560513.
19. Jiang, C.; Zhang, S. Power Quality Compensation Strategy of MMC-UPQC Based on Passive Sliding Mode Control. *IEEE Access* **2023**, *11*, 3662–3679. https://doi.org/10.1109/ACCESS.2022.3229893.
20. Kumar, U.; Kumar, S. Performance Evaluation of Shunt Active Power Filter for Aircraft System. *Int. Conf. Electr. Electron. Eng. ICE3 2020* **2020**, 370–375. https://doi.org/10.1109/ICE348803.2020.9122873.
21. Chaoui, A.; Gaubert, J.P.; Krim, F.; Champenois, G. PI Controlled Three-Phase Shunt Active Power Filter for Power Quality Improvement. *Electr. Power Components Syst.* **2007**, *35*, 1331–1344. https://doi.org/10.1080/15325000701426062.
22. Keerthi, Y.. Harmonic Elimination in a Three Phase System By Using D-Q Method. *Interantional J. Sci. Res. Eng. Manag.* **2023**, *07*, 1–11. https://doi.org/10.55041/ijsrem26996.
23. Mirjalili, S.; Lewis, A. The Whale Optimization Algorithm. *Adv. Eng. Softw.* **2016**, *95*, 51–67. https://doi.org/10.1016/j.advengsoft.2016.01.008.
24. Srivastava, A.; Das, D.K. A Whale Optimization Algorithm Based Shunt Active Power Filter for Power Quality Improvement. *Int. J. Electr. Energy* **2018**, *6*, 7–12. https://doi.org/10.18178/ijoee.6.1.7-12.
25. Iqbal, M.; Jawad, M.; Jaffery, M.H.; Akhtar, S.; Rafiq, M.N.; Qureshi, M.B.; Ansari, A.R.; Nawaz, R. Neural Networks Based Shunt Hybrid Active Power Filter for Harmonic Elimination. *IEEE Access* **2021**, *9*, 69913–69925. https://doi.org/10.1109/ACCESS.2021.3077065.
26. Salim, C. Five-Level (NPC) Shunt Active Power Filter Performances Evaluation Using Fuzzy Control Scheme for Harmonic Currents Compensation. *2017 6th Int. Conf. Syst. Control. ICSC 2017* **2017**, 561–566. https://doi.org/10.1109/ICoSC.2017.7958639.
27. Salleh, Z.M.T.; Alsammak, A.N.B.; Mohammed, H.A. Enhancing Power System Transient Stability Using Static VAR Compensator Based on a Fuzzy Logic Controller. *J. Eur. des Syst. Autom.* **2024**, *57*, 1565–1572. https://doi.org/10.18280/jesa.570603.

 doi:10.20944/preprints202605.0554.v1

28. Fawzy, I.Y.; Mossa, M.A.; Elsawy, A.M.; Suwarno, I.; Zaki Diab, A.A. Deployment of STATCOM with Fuzzy Logic Control for Improving the Performance of Power System under Different Faults Conditions. *J. Robot. Control* **2024**, *5*, 636–646. https://doi.org/10.18196/jrc.v5i3.21558.